Sediment transport prediction in sewer pipes during flushing operation

Montes, Carlos; Ortiz, Hachly; Vanegas, Sergio; Kapelan, Zoran; Berardi, Luigi; Saldarriaga, Juan

DOI
10.1080/1573062X.2021.1948077

Publication date
2021

Document Version
Accepted author manuscript

Published in
Urban Water Journal

Sediment Transport Prediction in Sewer Pipes During Flushing Operation

Carlos Montes[a*], Hachly Ortiz[b], Sergio Vanegas[c], Zoran Kapelan[d], Luigi Berardi[e] and Juan Saldarriaga[f]

[a]*Department of Civil and Environmental Engineering, Universidad de los Andes, Bogotá, Colombia; e-mail: cd.montes1256@uniandes.edu.co*

[b]*Department of Civil and Environmental Engineering, Universidad de los Andes, Bogotá, Colombia; e-mail: hv.ortiz@uniandes.edu.co*

[c]*Department of Civil and Environmental Engineering, Universidad de los Andes, Bogotá, Colombia; e-mail: sm.vanegas@uniandes.edu.co*

[d]*Department of Water Management, Delft University of Technology, Delft, Netherlands; e-mail: Z.Kapelan@tudelft.nl*

[e]*Department of Engineering and Geology, Università degli Studi "G. d'Annunzio" Chieti, Pescara, Italy; e-mail: luigi.berardi@unich.it*

[f]*Department of Civil and Environmental Engineering, Universidad de los Andes, Bogotá, Colombia; e-mail: jsaldarr@uniandes.edu.co*

*Corresponding author; Correspondence address: Cra 1 Este No. 19A – 40 Bogota (Colombia); Tel.: +57-1-339-49-49 (ext. 1765)

Sediment Transport Prediction in Sewer Pipes During Flushing Operation

Abstract

This paper presents a novel model for predicting the sediment transport rate during flushing operation in sewers. The model was developed using the Evolutionary Polynomial Regression Multi-Objective Genetic Algorithm (EPR-MOGA) methodology applied to new experimental data collected. Using the new model, a series of design charts were developed to predict the sediment transport rate and the required flushing operation time for several pipe diameters. Accurate results (i.e. sediment transport rates) were obtained when applied to a case study in a combined sewer pipe in Marseille, as reported in the literature. The novelty of the model is the inclusion of the pipe slope, the inflow "dam break" hydrograph, and the sediment properties as explanatory parameters. The new model can be used to predict flushing efficiency and design new flushing cleaning schedules in sewer systems.

Keywords: flushing efficiency; sediment transport; sewer cleansing; sewer flushing.

1. INTRODUCTION

Sediment deposition and accumulation are well-known issues in sewer systems modelling. The presence of permanent deposits of material at the bottom of sewer pipes produces several problems, such as reduced flow capacity and premature combined sewer overflows (Ashley et al. 2004; Rodríguez et al. 2012). Flushing waves, also known as surge flushing technique, have been identified as an efficient (Bong et al. 2016; Yang et al. 2019) and cost-effective (Campisano et al. 2019, 2007) method for solving these problems. It aims to remove the deposited sediments by generating waves, which are produced by the upstream storage and further discharge of water volumes. These flushing

43 waves increase the bottom shear stress and induce the scour and resuspension of the
44 deposited material.

45 The above flushing technique has been applied in several case studies following
46 operational and management practice guides (British Standard Institution, 2014; Fan,
47 2004; Hlavinek et al. 2005; NEIWPCC, 2003) in countries such as Germany, France, the
48 USA and the UK. As an example, Hlavinek et al. (2005) suggest flushing waves to
49 remove settled deposits in sewers ranging from 100 mm to 1200 mm pipe diameter with
50 a mandatory cleaning frequency once in 1 to 5 years. However, these guides do not
51 specify important flushing parameters such as the hydraulic and pipe characteristics (i.e.
52 length, slope and hydraulic roughness, among others), sediment properties and flushing
53 volume. The lack of information on these specifications has contributed to the fact that
54 existing flushing practices tend to be oversized. As an instance, Dettmar (2007) compared
55 design tables developed by using extensive field studies and mathematical simulations
56 (Chebbo et al. 1996; Dettmar, 2005; Lainé et al. 1998) and concluded that smaller
57 flushing volumes and water storage heights achieve the same flushing length and
58 efficiency in removing the volume of deposited sediments, compared to operational and
59 management practice guides.

60 In the last decades, several studies have quantified the flushing efficiency in terms
61 of: (a) reduction of volume and/or weight of sediments (Bong et al. 2016; Campisano et
62 al. 2019, 2008, 2004; Creaco and Bertrand-Krajewski, 2009; Guo et al. 2004; Ristenpart,
63 1998; Shahsavari et al. 2017), (b) changes in deposited bed thickness (Bong et al. 2016,
64 2013a; Campisano et al. 2019, 2008, 2007, 2004; Dettmar et al. 2002; Ristenpart, 1998;
65 Shahsavari et al., 2017; Shirazi et al. 2014), (c) variation of concentrations of total
66 suspended solids (Ristenpart, 1998; Sakakibara, 1996), (d) increase in the bottom shear

67 stress (Bertrand-Krajewski et al. 2003; Campisano et al. 2008; Campisano and Modica,
68 2003; Dettmar et al. 2002; Ristenpart, 1998; Schaffner and Steinhardt, 2006; Yang et al.
69 2019), (e) length of the channel that can be potentially cleaned (Bertrand-Krajewski et al.
70 2003; Bong et al. 2013; Dettmar et al. 2002; Shahsavari et al. 2017; Yang et al. 2019) and
71 (f) stored water volume discharged (Bertrand-Krajewski et al. 2003; Dettmar et al. 2002;
72 Fan et al. 2001). These studies were carried out in both laboratory and real sewer flumes
73 using different sediment characteristics, stored water volumes and geometrical
74 characteristics of the flume. As a result, a list of parameters affecting the flushing
75 efficiency was identified and classified in three main groups: (i) flushing hydraulics, (ii)
76 pipe geometry and (iii) sediment properties. Flushing hydraulic parameters include water
77 velocity (V_f), shear stress (τ), the water level in the pipe (Y), flowrate (Q), stored water
78 head (h_o) and stored water volume discharged (V_a). In the pipe geometry, parameters as
79 the slope (S_o), diameter (D), length (L), cross-section shape factor (β) and composite
80 roughness (k_c) have been included. Finally, sediment properties include mean particle
81 diameter (d), sediment thickness (y_s) and width (W_b), specific gravity (SG), porosity (η)
82 and density (ρ_s).

83 The previous three groups of parameters have been used for implementing
84 numerical models useful to quantify the flushing efficiency. Models found in the literature
85 are focused on (i) solving complex mathematical structures, (ii) proposing simple
86 dimensionless equations for estimating sediment transport rates and (iii) using Machine
87 Learning (ML) and Artificial Intelligence (AI) techniques for finding patterns in data and
88 predicting bedload and suspended load transport.

89 In the first approach, the one-dimensional Saint-Venant equations (Campisano et
90 al. 2006; Campisano and Modica, 2003; De Sutter et al. 1999), coupled with the Exner

equation for uniform (Campisano et al. 2007, 2004; Creaco and Bertrand-Krajewski, 2009; Shirazi et al. 2014) and non-uniform (Campisano et al. 2019) sediments, are used for predicting bed sediment thickness changes during the flushing operation. More complex models involve the two-dimensional (Caviedes-Voullième et al. 2017; Yu and Duan, 2014) and three-dimensional (Schaffner and Steinhardt, 2006) solutions of the Saint-Venant equations. An example of the literature models is as follows:

$$\frac{\partial U}{\partial t} + \frac{\partial F(U)}{\partial x} = D(U) \tag{1}$$

where U, $F(U)$ and $D(U)$ are defined as follows:

$$U = \begin{bmatrix} A \\ Q \\ A_s \end{bmatrix}; F(U) = \begin{bmatrix} Q \\ V_f Q + \frac{F_h}{\rho} \\ \frac{1}{1-\rho} Q_s \end{bmatrix}; D(U) = \begin{bmatrix} 0 \\ gA\left(S_o - \frac{{V_f}^2}{{k_c}^2 R^{4/3}}\right) \\ 0 \end{bmatrix} \tag{2}$$

where F_h is the hydrostatic force over the cross-section, ρ the water density, R the hydraulic radius, A is the cross section wetted area, A_s is the cross-section sediment bed area and Q_s the sediment flow rate.

In the second approach mentioned above, several authors have developed analytical equations for predicting the number of flushes required to move the deposited sediment bed (Bong et al. 2013; Chebbo et al. 1996). Likewise, the effects of pipe slope, bottom roughness, storage water level, and downstream water level, among others (Yang et al. 2019; Kuriqi et al. 2020) have also been studied in the past. As an example, Bong et al. (2013) proposed the following equation, where n_f is the number of flushes required to move the deposited sediment bed by 1 m:

$$n_f = 251.43 y_s + 6.57 \tag{3}$$

In the third approach, several studies using ML and AI have been developed for predicting both bedload and suspended load transport in sewers, flumes, and streams. Several techniques as Artificial Neural Networks (Wan Mohtar et al. 2018; Bajirao et al. 2021), Random Forests (Khosravi et al. 2020; Safari 2020; Montes et al. 2021), and Vector Machines (Ebtehaj et al. 2017), among others, have been trained with experimental data collected at laboratory scale and tested with benchmark data found in the literature. These models outperform traditional regression formulas during the training stage but tend to underperform when applied to external datasets collected in sewers and flumes (Montes et al. 2021), i.e. during the testing stage.

Numerical studies mentioned above, based on the solution of the Saint-Venant and Exner coupled-equations for sediment transport under unsteady flow conditions, show similar predictions of the sediment thickness changes compared to the experimental data collected, i.e. the models show good accuracy prediction. Despite the solutions and simulations based on Saint Venant-Exner equations showing good accuracy, in practice, the application for operational and management practices is complex and non-pragmatic. Also, the analytical and dimensionless equations proposed by Bong et al. (2013) and Yang et al. (2019), do not include important parameters such as the pipe/flume geometry and the sediment characteristics. Finally, AI and ML models are largely black-box models (Montes et al. 2021), limiting their interpretability for practical applications.

The above gaps are addressed here by developing a new parsimonious regression-based model using the Evolutionary Polynomial Regression – Multi-Objective Genetic Algorithm (EPR-MOGA) (Giustolisi and Savic, 2009) strategy. EPR-MOGA is a data-driven method which combines genetic algorithm with evolutionary computing for finding polynomial structures. Due to its characteristics, the returned symbolic

132 expressions can be compared with existing models in terms of the input variables,
133 exponent coefficients, and technical insight on the phenomenon (Montes et al. 2020a)
134 while reducing the risk of overfitting.

135 This paper aims to propose a new model for predicting the sediment transport rate
136 during flushing operations in sewers. The novelty of this model is the inclusion of
137 flushing "dam break" hydrograph, pipe geometry, and deposited sediment characteristics
138 in a simple polynomial expression. The new model developed here can be used to
139 optimize flushing schemes and reduce the volume of water required for cleaning sewers.

140 ## 2. EXPERIMENTAL METHODS AND DATA COLLECTION

141 The collection of experimental data was carried out in two pipes with diameters of 209
142 mm and 595 mm (Montes et al. 2020b), both located at the Hydraulics Laboratory of the
143 University of the Andes, Colombia. A sediment bed with a near-uniform thickness and
144 width was prepared at the bottom of the pipes, using uniformly graded sediment material
145 ranging from 0.21 mm to 2.6 mm. These particles had a specific gravity between 2.57
146 and 2.67, which was calculated using the pycnometer method (ASTM D854-14, 2014).
147 The experiments were carried out under unsteady flow conditions, simulating the "dam
148 break" waves produced during a flushing event. The methodology used for data collection
149 and further details of both experimental setups are described below.

150 ### *2.1. 209 mm pipe setup*

151 The 209 mm diameter acrylic pipe had a length of 10.58 m and was supported on six
152 hydraulic jacks, which allowed to vary the pipe slope between 0.64% and 1.20%. This
153 pipe was connected to a 200 mm solenoid valve, which controlled the inflow into the
154 setup from a 3.5 m^3 upstream tank. A downstream tank with a V-Notch weir was used to

155 measure the water discharge. A real-time water level sensor was used to measure the
156 water height over the weir to calculate the water discharge rate using the V-Notch
157 equation. The calculated discharge was also checked using an ABB- Electromagnetic
158 flowmeter sensor installed upstream of the pipe. Two additional real-time water level
159 sensors were installed along the pipe, aiming to measure the stage hydrograph produced
160 by the flushing waves. Figure 1 shows the general scheme of the experimental setup.

161 The experimental data was collected as follows. Firstly, the solenoid valve was
162 fully opened, allowing a base flowrate ranging from 0.002 l s^{-1} to 0.414 l s^{-1}. The opening
163 of this valve simulates the 'dam break hydrograph' produced during a flushing operation
164 in a real sewer pipe (e.g. using a Hydrass or a Hydroself flushing gate). Secondly, a
165 sediment bed with near-uniform thickness and width was located at the bottom of the
166 pipe. At this point, the base flowrate helped the formation of the deposited bed along a
167 3.3 m section. Thirdly, the solenoid valve was completely closed for storing a volume of
168 water between 0.10 m^3 and 0.31 m^3 in the upstream tank. Fourthly, the solenoid valve
169 was opened between 60% and 100% and the opening time was set to 15 sec for all tests.
170 When the first discharged wave reached the sediment bed, the movement of the bed was
171 tracked over time. The sediment velocity (V_s) was calculated using the values of the time
172 and deposited bed displacement during the peak flow. The above procedure was repeated
173 for different accumulated upstream water volume and percentage of the solenoid valve
174 opening.

175 **[Figure 1 near here]**

176 ***2.2. 595 mm pipe setup***

177 The pipe was 10.5 m long and supported on a mechanical steel truss, which allowed to
178 modify the slope in a range between 0.04% and 3.44%. The base flow for the experiments,

ranging from 1.03 l s^{-1} to 9.98 l s^{-1}, was provided by a 40 BHP pump that supplied water to a 30 m^3 upstream storage which was directly connected to the pipe. For evaluating unsteady flow conditions in this pipe, a second 10 BHP submersible pump was located inside the downstream tank. This pump was directly connected to the upstream tank and was controlled with a variable frequency drive programmed before the experiment to create a pulse with a maximum peak flow of 30 l s^{-1}. Three water level sensors were used to record water depths in the experimental setup. Two of them were installed in the pipe to collect the stage hydrograph, and one was installed in the upstream tank. Full details of the experimental setup were described in Montes et al. (2020b) and are shown in Figure 2.

[Figure 2 near here]

For this setup, the data was collected as follows. Firstly, the pipe slope was adjusted using the mechanical steel truss and measured with a dumpy level. Secondly, the flow control valve on the upstream tank was opened to supply a base flow to the pipe. Thirdly, a deposited sediment bed with a near-uniform width was prepared at the bottom of the pipe over a minimum length of 1.5 m. At this point, to compare the flushing efficiency under similar conditions, the maximum sediment bed velocity was verified as 0.03 m s^{-1}. If this condition was not fulfilled, the pipe slope or the base flow were changed. Fourthly, the submersible pump, with its variable frequency drive, was activated to simulate the 'dam break hydrograph', which is similar to those produced by the flushing gates in real sewers. The water levels were recorded each 0.025 sec and the position of the sediment bed was tracked. The sediment velocity was calculated using the same procedure followed on the acrylic setup.

2.3. Experimental data collected

Using the experimental rig and approach described above, a total of 57 and 64 experiments were carried out in the 209 mm acrylic pipe and 595 mm PVC pipe, respectively. Several variables related to the pipe geometry, sediment properties, and flushing hydraulics, including the base time (t_b), peak time (t_p), base flow (Q_b), and peak flow (Q_p) were recorded in each experiment, as shown in Figure 3. The experimental data collected in both acrylic and PVC pipes are presented in Table 1, where S_o is the pipe slope, D the pipe diameter, Y the water level in the pipe, R the hydraulic radius, d the mean particle diameter, SG the specific gravity, y_s the sediment thickness, V_f the water velocity, and V_s the sediment velocity.

[Figure 3 near here]

[Table 1 near here]

A flushing discharge hydrograph and a plot showing the sediment bed position related with each run are presented in Table 1. The shape and magnitude of the hydrograph are directly related to the sediment bed velocity, and consequently, the sediment bed position. As an example, for six runs, the variation in the sediment bed position and hydrograph characteristics, in both acrylic and PVC pipe, are presented in Figure 4. Full details of each run shown in Figure 4 are presented in Table 1.

[Figure 4 near here]

Figure 4A and Figure 4B show the relation between the flushing discharge hydrograph and the sediment bed position for tests conducted on the acrylic pipe. As seen in these figures, particle size is a more important variable in defining the sediment position, compared to the peak flow in the hydrograph. Even though the run 82 considers

225 a higher peak flow (Q_p = 5.55 l s^{-1}), the final position of the sediment bed (= 0.41 m) is
226 lower than the run 96 (= 2.62 m) when the peak flow is lower (Q_p = 2.08 l s^{-1}). This occurs
227 because the particle diameter is more relevant compared to the peak flow.

228 Figure 4C and Figure 4D show the relation between the flushing discharge
229 hydrograph and the sediment bed position for tests in 595 mm setup. The relationship
230 between the discharge hydrograph and the sediment bed position is proportional. For run
231 no. 36 and 61, the mean particle diameter was 2.60 mm, but the pipe slope was 1.65%
232 and 1.82%, respectively. Figure 4D shows that maintaining the mean particle diameter
233 constant as the pipe slope increases, the final bed position increases.

234 **3. MODEL DEVELOPMENT**

235 ***3.1. Graphical analysis***

236 A graphical analysis was developed to visualize the relationships between the variables
237 collected in each experiment. The relationship between sediment velocity and flow
238 velocity (V_s/V_f) was plotted against other dimensionless parameters, as shown in Figure
239 5. These dimensionless parameters have been previously identified as relevant for
240 predicting sediment transport in sewer pipes in previous literature (Ab Ghani and
241 Azamathulla, 2011; Ebtehaj and Bonakdari, 2016; May et al. 1996; Kuriqui et al. 2020;
242 Montes et al. 2021). Two of these parameters include the dimensionless grain size (d/R)
243 and the Shields parameter (ψ), defined in Eq. (4):

$$\psi = \frac{RS_o}{(SG-1)d} \tag{4}$$

244 Based on the results shown in Figure 5, the following observations can be made:

- In general, higher values of the Shields parameter lead to higher values of V_s/V_f. This can be clearly seen in the acrylic pipe (Figure 5a) because of the constant slope value adopted in the experimental rig. Furthermore, high values of S_o and R lead to higher sediment velocities due to higher critical shearing stress (i.e. the applied forces are higher than the submerged weight of the particle). In contrast, deposited materials with high density of particle diameters result in lower sediment velocities.
- The direct relationship between V_s/V_f and the Shields parameter coincides with the inversely proportional relationship between V_s/V_f and d/R, shown in Figure 5c and Figure 5d. This is observed because the Shields parameter includes the ratio R/d, as shown in Eq. (4).
- Figure 5e shows the inversely proportional relationship between V_s/V_f and the dimensionless parameter Q_b/Q_p, meaning that higher and steeper discharge hydrographs (i.e. lower ratios Q_b/Q_p) show higher V_s/V_f values.
- In general, based on what was previously mentioned, higher values of S_o and R and lower values of d, SG, and Q_b/Q_p lead to higher sediment velocities V_s.

[Figure 5 near here]

3.2. Evolutionary Polynomial Regression model

A new regression-based model was developed here to predict the dimensionless ratio V_s/V_f during flushing operation. The new model includes the group of parameters identified in previous studies (Ab Ghani and Azamathulla, 2011; Ebtehaj and Bonakdari, 2016; May et al. 1996; Montes et al. 2021) and the graphic analysis carried out for the experimentally collected data, as shown in Figure 5.

Evolutionary polynomial regression (EPR) is a hybrid regression technique that combines numerical and symbolic regression (Giustolisi and Savic, 2006, 2004). In its original formulation, it used single objective genetic algorithms to explore the formula space, and then it estimates the least-squares regression coefficients. This technique has proved to be effective when the number of polynomial terms is not large (Giustolisi and Savic, 2009). To solve these issues, Giustolisi and Savic (Giustolisi and Savic, 2009) introduced the EPR technique combined with a Multi-Objective Genetic Algorithm (MOGA). This novel technique maximises the model accuracy (i.e. minimises the sum of squared errors) and minimises the number of polynomial coefficients, and therefore improves the exploration of the space of symbolic formulas. EPR-MOGA considers some pseudo-polynomial expressions such as (Giustolisi and Savic, 2009):

$$\widehat{\boldsymbol{Y}} = a_0 + \sum_{j=1}^{m} a_j (\boldsymbol{X_1})^{ES(j,1)} \cdot \ldots \cdot (\boldsymbol{X_k})^{ES(j,k)} \cdot f\left((\boldsymbol{X_1})^{ES(j,k+1)}\right) \cdot \ldots \cdot f\left((\boldsymbol{X_k})^{ES(j,2k)}\right) \qquad (5)$$

where $\widehat{\boldsymbol{Y}}$ is the vector of model predictions; ES and j the matrix of candidate exponents and the inner function, respectively, both selected by the user; m the number of terms; a_0 the bias term; a_j the adjustable parameters estimated by linear least squares and $\boldsymbol{X_j}$ the candidate explanatory variables. The inner function f defined by the user can be logarithmic, exponential, tangent hyperbolic, or secant hyperbolic, and must be selected according to the physics of the problem studied. The EPR technique returns a range of models showing the influence of different explanatory factors by progressively adding these as input variables to monomial formulas, starting from the most important ones. For each EPR identified model, the following performance indices are calculated: the Bayesian Information Criterion (BIC) and the Coefficient of Determination (R^2), as shown in Eq. (6) and Eq. (7), respectively.

$$BIC = \left(1 + d\frac{\log(n)}{n}\right)\left(\sum_{i=1}^{n}(Y^* - Y)^2\right) \quad (6)$$

$$R^2 = 1 - \frac{\sum_{i=1}^{n}(Y^* - Y)^2}{\sum_{i=1}^{n}(Y^* - \overline{Y^*})^2} \quad (7)$$

where Y^* and Y are the observed and calculated data, respectively, n is the number of data, d the number of parameters included in the model and $\overline{Y^*}$ the mean of observed data. The Coefficient of Determination measures the fraction of variance that can be explained. Note that this coefficient varies between 0 and 1, where 1 denotes a perfect match between observed and calculated data. The Bayesian Information Criterion measures the trade-off between accuracy and parsimony of the model. This measure penalises formulas with large number of parameters. The model with the lowest BIC value is selected as optimal.

The new model was constructed to predict the dimensionless relation V_s/V_f, i.e. the vector of model predictions $\widehat{\boldsymbol{Y}}$ is defined as V_s/V_f. The matrix of candidate exponents was defined with values ranging from -2.50 to 2.50, considering steps of 0.1, i.e. $ES = [-2.50, -1.40, \ldots, 1.40, 2.50]$. The matrix of candidate explanatory variables is defined as follows:

$$\boldsymbol{X_j} = \left[\psi, \frac{d}{R}, \frac{Q_b}{Q_p}, \frac{y_s}{R}, \frac{t_b}{t_p}, \beta\right] \quad (8)$$

Using previous considerations, and randomly splitting the experimental data collected on the 209 mm and 595 mm pipes, for both training (75% of the data) and testing (25% of the data) stages, the results shown in Table 2 were obtained using the EPR-MOGA strategy.

[Table 2 near here]

Table 2 shows the Pareto front (i.e. range of models) generated by the EPR, together with the corresponding BIC and R^2 values. For example, the best 1 input variable model includes only the Shields parameter as an explanatory variable for predicting the V_s/V_f ($V_s/V_f = 0.17\psi^{0.5}$). This is the least complex, i.e. most parsimonious model hence, unsurprisingly, it has a rather low prediction accuracy (BIC = -48.21 and R^2 = 0.38). In contrast, the 6-variable model includes all candidate explanatory factors $\left(V_s/V_f = 2.48\psi^{1.4}\left(\frac{Q_b}{Q_p}\right)^{-0.3}\left(\frac{d}{R}\right)^{0.9}\left(\frac{y_s}{R}\right)^{0.1}\left(\frac{t_b}{t_p}\right)^{-0.2}\beta\right)$, resulting in low parsimony model but with improved prediction accuracy (BIC = -92.22 and R^2 = 0.64). Based on this, the model that shows the best trade-off between accuracy and parsimony is the model with 3 input variables. This model is shown in Eq. (9).

$$\frac{V_s}{V_f} = 8.13\left(\frac{d}{R}\right)^{0.90}\left(\frac{RS_o}{(SG-1)d}\right)^{1.40}\left(\frac{Q_b}{Q_p}\right)^{-0.30} \quad (9)$$

Or rearranging the above formula to simplify the d/R term:

$$\frac{V_s}{V_f} = 8.13\left(\frac{d}{R}\right)^{-0.50}\left(\frac{S_o}{(SG-1)}\right)^{1.40}\left(\frac{Q_b}{Q_p}\right)^{-0.30} \quad (10)$$

The obtained model was used to estimate the flushing efficiency in larger pipes considering different flow conditions and sediment characteristics. Further details are described in the section below. The model's accuracy can be seen in Figure 6 for both training and testing datasets.

[Figure 6 near here]

As it can be seen from the above equation and figure, Eq. (10) is consistent with the graphical analysis presented in Figure 6. Further, it can be seen from the model obtained that $\frac{S_o}{(SG-1)}$ is the most important feature for predicting the sediment velocity

during the flushing cleaning operation - the more the pipe slope increases, the higher the particle velocity is (note that the $\frac{S_o}{(SG-1)}$ parameter comes from the Shields parameter). The Shields parameter shows the ratio between the hydrodynamic forces acting on the particles and the resistance due to gravity. This parameter has been identified as one of the most relevant for predicting the incipient motion in sewers (Delleur, 2001; Safari et al. 2018; Wan Mohtar et al. 2018). As mentioned above, V_s/V_f is inversely proportional to d/R, which is consistent with the results shown by EPR-MOGA model.

4. RESULTS AND DISCUSSION

The new model shown in Eq. (10) was used to generate charts to estimate flushing efficiency as a function of the characteristics of the discharged hydrograph, the pipe geometry and the sediment properties. In this context, two flushing-efficiency measures were defined as a function of the area of deposited bed (A_s) and the sediment velocity. The first measure, Q_s, is the volume of sediment removed by unit time (i.e. the sediment flow rate = $A_s V_s$). The second measure, t_e, is the flushing time required to clean 1.0 m of the pipe (= $1/V_s$). Figure 7 and Figure 8 were constructed for several pipe diameters using previous measures. To construct these figures, the less-significant variables identified by the EPR-MOGA model (as shown in Table 2) remained constant. The sediment thickness was defined as $y_s/D = 1\%$, the specific gravity of the sediments as 2.6, and the relation between the base and peak time of the hydrograph as $t_b/t_p = 5.0$.

[Figure 7 near here]

The following observations can be made from Figure 7 and Figure 8:

- Q_s is inversely proportional to d and Q_b/Q_p. In addition, Q_s seems to be near-steady for particle diameters greater than 1.5 mm in pipes with diameters less than

800 mm. All above for the same pipe slope and Q_b/Q_p relation. Increasing the pipe slope directly increase the sediment transport rate.

- As the Q_b/Q_p ratio increases, the sediment removal rate decreases. For example, in Figure 7a, when Q_b/Q_p = 0.25 in a 1200 mm diameter pipe containing a deposited sediment bed with d = 1 mm, Q_s = 0.5 $\times 10^{-4}$ m^3/s, while for Q_b/Q_p = 0.75 the Q_s value changes to 0.2 $\times 10^{-4}$ m^3/s, that is 60% less (as shown in Figure 7c).
- Flushing discharges seem to be more efficient in larger sewer pipes. The sediment transport rate can be five times higher in 2000 mm diameter pipes, compared to 1200 mm diameter pipes.
- Figure 8 shows a direct relationship between t_e and d and Q_b/Q_p. Based on this, as d increases and Q_p decreases, the required flushing time to clean 1 meter of the pipe increases. For example, in Figure 8d when Q_b/Q_p = 0.25 in a 800 mm diameter pipe containing a deposited sediment bed with d = 1.5 mm, t_e = 20 sec, while for Q_b/Q_p = 0.75 the t_e value changes to 45 sec, that is 125% more (as shown in Figure 8f)
- The flushing time decreases as the S_o and D increase. That is, flushing is a more efficient technique in large and steep pipes.

[Figure 8 near hear]

4.1. Model comparison

To test the accuracy of the model shown in Eq. (10), the case study described in Laplace et al. (2003) was used. This case study is located in Marseille, France, on a combined sewer network. Specifically, this study considers an ovoid section of 1700 mm, 120 m long with a bottom slope of 0.03%. A near-uniform deposited bed of 140 mm thickness

was observed along the entire length of the flume. The deposited bed was characterised as coarser upstream (d = 8 mm) and finer downstream (d = 0.6 mm). Full details are shown in Laplace et al. (2003).

Using a Hydrass-flushing gate located inside the section, a series of flushes were conducted for testing the efficiency on removing the deposited material. During each flush, a total volume of 6.0 m^3 of water was discharged into the pipe. As reported by Laplace et al. (2003), the mass of particles eroded during the first flush was 6.3 kg, i.e. the removal rate was 1.08 kg of material per 1.0 m^3 of water (= 1.08 kg m^{-3}).

Two existing procedures are compared with the new EPR-MOGA model presented in Eq. (10): the model proposed by Bong et al. (2013) (i.e. Eq. (3)) and the design tables shown by Dettmar (2007). To compare the results, several initial conditions are defined based on the case study description, which are outlined as follows:

(1) Thickness of the deposited bed (y_s) = 0.14 m

(2) Peak flow during flushing operation (Q_p) = 100 l s^{-1}

(3) Specific gravity of the sediments (SG) = 2.60

(4) Mean particle diameter (d) = 0.6 – 8.0 mm

(5) Mass of material per meter of pipe = 54.22 kg m^{-1}

According to Bong et al. (2013), the number of flushes required to move 1 m of deposited material can be estimated by applying Eq. (3). For this equation, the number of flushes is only a function of the thickness of the deposited bed. As a result, 42 flushes (= 250.6 m^3 of water) can potentially remove 54.22 kg of the deposited material (i.e. the removal rate is 0.21 kg m^{-3}). Design tables proposed by Dettmar (2007) suggest a flushing

396 volume of 48 m^3 for a basic cleaning of the 150 m long sewer (i.e. a full removing of the
397 deposited material). No removal rates are provided by Dettmar (2007).

398 Finally, using the new model proposed in this study, a range of removal rates are
399 obtained as a function of the mean particle diameter. Potentially, a flushing volume of
400 10.18 m^3 can remove 14.5 kg of deposited material with a mean particle diameter of 0.6
401 mm (i.e. the removal rate is 0.40 kg m^{-3}). By changing the particle size of the deposited
402 material to 8.3 mm, the removal rate is 1.25 kg m^{-3}.

403 **[Table 3 near here]**

404 As shown in Table 3, a direct comparison of the method proposed by Dettmar
405 (2007) and the results reported by Laplace et al. (2003) is not possible. However, this
406 method seems to underestimate the real volume required to remove the deposited bed.
407 Relevant parameters such as the mean particle diameter and the sewer hydraulics are not
408 included in this method. Due to the pipe slope in the case of study is almost flat, obtaining
409 minimum shear stress of 5.0 N m^{-2} for cleaning the pipe, according to Dettmar (2007),
410 requires larger flows.

411 The model presented by Bong et al. (2013) is a good approach for determining the
412 number of flushes required to move the deposited material. However, because of the non-
413 inclusion of relevant pipe hydraulics and sediment parameters, the results are
414 underestimated, compared to the values reported by Laplace et al. (2003).

415 ***4.2. Model considerations***

416 The new model presented here shows good prediction accuracy with the data
417 reported by Laplace et al. (2003). This is explained by the inclusion of relevant parameters
418 for predicting the removal rate during the flushing operation. The model also shows good

419 extrapolation capabilities under different sewer diameters and a wide range of variations
420 of the mean particle diameter.

421 The Shields parameter was selected as the most important one due to the highest
422 value in the regression coefficient and the Pareto solution provided by the EPR-MOGA
423 strategy. This was expected since this parameter determines the threshold condition of
424 sediment initiation motion. The sediment thickness parameter is less important for
425 defining the sediment velocity during the flushing operation due to the low regression
426 coefficient presented in Table 2. As a result, the model can be used in both combined and
427 storm sewers, where the sediment thickness ranges from 10 mm to 100 mm and 10 mm
428 to 330 mm, respectively (Bong et al. 2016).

429 The model includes the peak flow as an explanatory variable for predicting
430 sediment transport rate. Higher peak flow implies a higher removal rate since higher shear
431 stresses are generated at the bottom of the pipe. The observed shear stress values (ranging
432 from 2.0 N/m^2 to 6.5 N/m^2 in the PVC pipe) are consistent with those reported in the
433 literature for the erosion and transport of bed material (Dettmar, 2007; Campisano et al.
434 2008; Yang et al. 2019). However, since the model only considers transport as bedload,
435 some fine particles may be eroded and transported in suspension (which has been
436 identified as one of the major sources of pollution in CSO (Laplace et al. 2003; Saul et
437 al. 2003)), due to the high turbulence of the flow. This is particularly important in well-
438 graded materials where wide ranges of mean particle sizes are present.

439 Even though the new model was developed considering a wide range of variations
440 in input variables, some limitations exist. The granular material used in the experiments
441 cannot represent the cohesive properties of sediments found in real sewer systems. As a
442 result, an increased bed resistance to erosion can be seen in practice (Campisano et al.

2019). In addition, the lowest pipe slope value considered during the tests was 0.644%, which is higher than the minimum self-cleansing value recommended in several industry design codes and water utilities design manuals (e.g. Health Research Inc. (2004), as quoted by Montes et al. (2019)).

5. CONCLUSIONS

This study proposes a simple model to predict the sediment transport rate in practice based on data collected from a set of 121 lab experiments conducted on a 209 mm diameter acrylic pipe and 595 mm diameter PVC pipe. The data collected this way were processed using the EPR-MOGA modelling technique. A new model for predicting the sediment velocity during flushing operation was developed and used for constructing design charts. Based on the results obtained, the following conclusions are made:

(1) The new model developed and presented here can predict the sediment transport rate during flushing discharges accurately in practice. This model includes the group of parameters that most affect the flushing efficiency in sewer pipes.

(2) The sediment transport rate is principally affected by four parameters: pipe slope, pipe diameter, particle diameter and discharged peak flow. In pipes with large diameters and slopes, the flushing is more effective. This is because of the high regression exponents for both $\frac{S_o}{(SG-\ )}$ and d/R variables obtained in the EPR-MOGA model presented here. The sediment transport is not significantly affected by the value of the deposited sediment thickness.

(3) The new model proposed outperforms the simplified models and methods reported in the literature in terms of removal sediment rate prediction. This is seen by the better prediction accuracy shown when compared to the case study reported by Laplace et al. (2003).

(4) Existing models such as Bong et al. (2013) and Dettmar (2007) for predicting sediment transport tend to underestimate the total volume of water required to clean a deposited sediment bed. The EPR-MOGA model is more accurate in predicting the sediment transport rate as this model includes parameters affecting the flushing efficiency, such as flushing hydraulics, pipe geometry and sediment properties.

Based on the conclusions mentioned above, the new flushing model can be useful for designing flushing schemes during the operational stage of existing sewer pipes in engineering practice. Further research is recommended to test the model proposed in real sewer pipes under different sediment (i.e. cohesive materials) and hydraulic conditions.

Acknowledgements

The authors would like to thank Professor Orazio Giustolisi who developed and made available for free the EPR software used in this research.

Disclosure Statement

No potential conflict of interest was reported by the author(s).

Funding

This research received no external funding.

REFERENCES

Ab Ghani, A., and Azamathulla, H. 2011. "Gene-Expression Programming for Sediment Transport in Sewer Pipe Systems." *Journal of Pipeline Systems Engineering and Practice* 2(3): 102–106. https://doi.org/10.1061/(ASCE)PS.1949-1204.0000076

Ashley, R., Bertrand-Krajewski, J., Hvitved-Jacobsen, T., and Verbanck, M., 2004. *Solids in Sewers: Characteristics, Effects and Control of Sewer Solids and Associated Pollutants*. London: IWA Publishing. https://doi.org/10.2166/9781780402727

ASTM D854-14, 2014. *Standard Test Methods for Specific Gravity of Soil Solids by*

Water Pycnometer. West Conshohocken, PA: ASTM International.

Azamathulla, H., Ab Ghani, A., and Fei, S., 2012. "ANFIS-based approach for predicting sediment transport in clean sewer." *Applied Soft Computing Journal* 12(3): 1227–1230. https://doi.org/10.1016/j.asoc.2011.12.003

Bajirao, T., Kumar, P., Kumar, M., Elbeltagi, A., and Kuriqi, A. 2021. "Superiority of Hybrid Soft Computing Models in Daily Suspended Sediment Estimation in Highly Dynamic Rivers." *Sustainability* 13(2): 542. https://doi.org/10.3390/su13020542

Bertrand-Krajewski, J., Bardin, J., Gibello, C., and Laplace, D. 2003. "Hydraulics of a sewer flushing gate." *Water Science and Technology* 47(4), 129–136. https://doi.org/10.2166/wst.2003.0237

Bong, C., Lau, T., and Ab Ghani, A. 2016. "Potential of tipping flush gate for sedimentation management in open stormwater sewer." *Urban Water Journal* 13(5): 486–498. https://doi.org/10.1080/1573062X.2014.994002

Bong, C., Lau, T., Ab Ghani, A., and Chan, N. "Sediment deposit thickness and its effect on critical velocity for incipient motion." *Water Science and Technology* 74(8): 1876-1884. https://doi.org/10.2166/wst.2016.376

Bong, C., Lau, T., and Ab Ghani, A. 2013. "Hydraulics characteristics of tipping sediment flushing gate." *Water Science and Technology* 68(11): 2397–2406. https://doi.org/10.2166/wst.2013.498

British Standard Institution, 2014. *Management and Control of Operational Activities in Drain and Sewer Systems Outside Buildings. Part 1: Cleaning*. London, UK.

Campisano, A., Creaco, E., and Modica, C. 2008. "Laboratory investigation on the effects of flushes on cohesive sediment beds." *Urban Water Journal* 5(1): 3–14. https://doi.org/10.1080/15730620701726259

Campisano, A., Creaco, E., and Modica, C. 2007. "Dimensionless Approach for the Design of Flushing Gates in Sewer Channels." *Journal of Hydraulic Engineering* 133(8): 964–972. https://doi.org/10.1061/(ASCE)0733-9429(2007)133:8(964)

Campisano, A., Creaco, E., and Modica, C. 2006. "Experimental analysis of the hydrass flushing gate and laboratory validation of flush propagation modelling." *Water Science and Technology* 54(6-7): 101–108. https://doi.org/10.2166/wst.2006.608

Campisano, A., Creaco, E., and Modica, C. 2004. "Experimental and numerical analysis of the scouring effects of flushing waves on sediment deposits." *Journal of Hydrology* 299(3-4): 324–334. https://doi.org/10.1016/j.jhydrol.2004.08.009

Campisano, A., and Modica, C. 2003. "Flow velocities and shear stresses during flushing operations in sewer collectors." *Water Science and Technology* 47(4): 123–128. https://doi.org/10.2166/wst.2003.0236

Campisano, A., Modica, C., Creaco, E., and Shahsavari, G. 2019. "A model for non-uniform sediment transport induced by flushing in sewer channels." *Water Research* 163: 114903. https://doi.org/10.1016/j.watres.2019.114903

Caviedes-Voullième, D., Morales-Hernández, M., Juez, C., Lacasta, A., and García-Navarro, P. 2017. "Two-dimensional numerical simulation of bed-load transport of a finite-depth sediment layer: Applications to channel flushing." *Journal of Hydraulic Engineering* 143(9):04017034. https://doi.org/10.1061/(ASCE)HY.1943-7900.0001337

Chebbo, G., Laplace, D., Bachoc, A., Sanchez, Y., and Le Guennec, B. 1996. "Technical solutions envisaged in managing solids in combined sewer networks." *Water Science and Technology* 33(9): 237–244. https://doi.org/10.1016/0273-1223(96)00392-7

Creaco, E., and Bertrand-Krajewski, J. 2009. "Numerical Simulation of flushing effect on sewer sediments and comparison of Four sediment transport formulas." *Journal of Hydraulic Research* 47(2): 195–202. https://doi.org/10.3826/jhr.2009.3363

De Sutter, R., Huygens, M., and Verhoeven, R. 1999. "Unsteady flow sediment transport in a sewer model." *Water Science and Technology* 39(9): 121–128. https://doi.org/10.1016/S0273-1223(99)00224-3

Delleur, J. 2001. "New results and research needs on sediment movement in urban drainage." *Journal of Water Resources Planning and Management* 127(3): 186-193. https://doi.org/10.1061/(ASCE)0733-9496(2001)127:3(186)

Dettmar, J. 2007. "A new planning procedure for sewer flushing." Paper presented at the NOVATECH 2007 – Sixth International Conference on Sustainable Techniques and Strategies in Urban Water Management, Lyon, June 25-28.

Dettmar, J. 2005. "Beitrag zur Verbesserung der Reinigung von Abwasserkanälen." PhD diss., RWTH Aachen University.

Dettmar, J., Rietsch, B., and Lorenz, U. 2002. "Performance and Operation of Flushing Devices - Results of a Field and Laboratory Study." *Global Solutions for Urban Drainage: Proceedings of the Ninth International Conference on Urban Drainage*: 1–10. https://doi.org/10.1061/40644(2002)291

Ebtehaj, I., and Bonakdari, H. 2016. "Bed Load Sediment Transport in Sewers at Limit of Deposition." *Scientia Iranica* 23(3): 907–917. https://doi.org/10.24200/sci.2016.2169

Ebtehaj, I., Bonakdari, H., Shamshirband, S., Ismail, Z., and Hashim, R. 2017. "New approach to estimate velocity at limit of deposition in storm sewers using vector machine coupled with firefly algorithm." *Journal of Pipeline Systems Engineering and Practice* 8(2): 04016018. https://doi.org/10.1061/(ASCE)PS.1949-1204.0000252

Fan, C. 2004. *Sewer Sediment and Control A Management Practices Reference Guide*. U.S. Environmental Protection Agency, Washington, DC, EPA/600/R-04/059.

Fan, C., Field, R., Pisano, W., Barsanti, J., Joyce, J., and Sorenson, H. 2001. "Sewer and Tank Flushing for Sediment, Corrosion, and Pollution Control." *Journal of Water Resources Planning and Management* 127(3): 194–201.

https://doi.org/10.1061/(ASCE)0733-9496(2001)127:3(194)

Giustolisi, O., and Savic, D. 2009. "Advances in data-driven analyses and modelling using EPR-MOGA." *Journal of Hydroinformatics* 11(3-4): 225–236. https://doi.org/10.2166/hydro.2009.017

Giustolisi, O., and Savic, D. 2006. "A symbolic data-driven technique based on evolutionary polynomial regression." *Journal of Hydroinformatics* 8(4): 207–222. https://doi.org/10.2166/hydro.2006.020

Giustolisi, O., and Savic, D. 2004. "A Novel Genetic Programming Strategy: Evolutionary Polynomial Regression." *Proceedings of the 6th International Conference on Hydroinformatics*: 787–794. https://doi.org/10.1142/9789812702838_0097

Guo, Q., Fan, C., Raghaven, R., and Field, R. 2004. "Gate and Vacuum Flushing of Sewer Sediment: Laboratory Testing." *Journal of Hydraulic Engeneering* 130(5): 463–466. https://doi.org/10.1061/(ASCE)0733-9429(2004)130:5(463)

Health Research Inc. (2004). "Recommended standards for wastewater facilities." *A Report of the Wastewater Committee* 12224(518): 1–102.

Hlavinek, P., Malanik, S., Raclavsky, J., Sulcova, V., Montero, C., and Villanueva, A. 2005. *WP4 Deliverable 11: Survey of Operational Options*. Brno.

Khosravi, K., Cooper, J., Daggupati, P., Thai Pham, B., and Tien Bui, D. 2020. "Bedload transport rate prediction: Application of novel hybrid data mining techniques" *Journal of Hydrology* 585: 124774 https://doi.org/10.1016/j.jhydrol.2020.124774

Kuriqui, A., Koçileri, G., and Ardiçlioğlu, M. 2020. "Potential of Meyer-Peter and Müller approach for estimation of bed-load sediment transport under different hydraulic regimes" *Modeling Earth Systems and Environment* 6: 129-137. https://doi.org/10.1007/s40808-019-00665-0

Lainé, S., Phan, L., Malabat, D., and Duffros, B. 1998. "Flush Cleaning of Sewer Using the Hydras-Valve." Paper presented at the 4th International Conference on Urban Drainage Modelling, London, September 21-24.

Laplace, D., Oms, C., Ahyerre, M., Chebbo, G., Lemasson, J., and Felouzis, L. 2003. "Removal of the organic surface layer in combined sewer sediment using a flushing gate." *Water Science and Technology* 47(4): 19–26. https://doi.org/10.2166/wst.2003.0211

May, R., Ackers, J., Butler, D., and John, S. 1996. "Development of design methodology for self-cleansing sewers." *Water Science and Technology* 33(9): 195–205. https://doi.org/10.1016/0273-1223(96)00387-3

Montes, C., Bohorquez, J., Borda, S., and Saldarriaga, J. 2019. "Impact of Self-Cleansing Criteria Choice on the Optimal Design of Sewer Networks in South America." *Water (Switzerland)* 11(6): 1148. https://doi.org/10.3390/w11061148

Montes, C., Berardi, L., Kapelan, Z., and Saldarriaga, J. 2020a. "Predicting bedload

610 sediment transport of non-cohesive material in sewer pipes using evolutionary
611 polynomial regression – multi-objective genetic algorithm strategy." *Urban Water*
612 *Journal* 17(2): 154-162. https://doi.org/10.1080/1573062X.2020.1748210

613 Montes, C., Vanegas, S., Kapelan, Z., Berardi, L., and Saldarriaga, J. 2020b. "Non-
614 deposition self-cleansing models for large sewer pipes." *Water Science and*
615 *Technology* 81(3): 606–621. https://doi.org/10.2166/wst.2020.154

616 Montes, C., Kapelan, Z., and Saldarriaga, J. 2021. "Predicting non-deposition sediment
617 transport in sewer pipes using Random forest." *Water Research* 189, 116639.
618 https://doi.org/10.1016/j.watres.2020.116639

619 NEIWPCC, 2003. Optimizing Operation, Maintenance, and Rehabilitation of Sanitary
620 Sewer Collection Systems. Lowell, MA.

621 Ristenpart, E. 1998. "Solids transport by flushing of combined sewers." *Water Science*
622 *and Technology* 37(1): 171–178. https://doi.org/10.1016/S0273-1223(97)00767-1

623 Rodríguez, J., McIntyre, N., Díaz-Granados, M., and Maksimović, Č. 2012. "A database
624 and model to support proactive management of sediment-related sewer blockages."
625 *Water Research* 46(15): 4571–4586. https://doi.org/10.1016/j.watres.2012.06.037

626 Safari, M. 2020. "Hybridization of multivariate adaptive regression splines and random
627 forest models with an empirical equation for sediment deposition prediction in open
628 channel flow." *Journal of Hydrology* 590: 125392.
629 https://doi.org/10.1016/j.jhydrol.2020.125392

630 Safari, M., Mohammadi, M., and Ab Ghani, A. 2018. "Experimental studies of self-
631 cleansing drainage system design: A review." *Journal of Pipeline Systems*
632 *Engineering and Practice* 9(4): 04018017. https://doi.org/10.1061/(ASCE)PS.1949-
633 1204.0000335

634 Sakakibara, T. 1996. "Sediments flushing experiment in a trunk sewer." *Water Science*
635 *and Technology* 33(9): 229–235. https://doi.org/10.1016/0273-1223(96)00391-5

636 Saul, A., Skipworth, P., Tait, S., and Rushforth, P. 2003. "Movement of Total Suspended
637 Solids in Combined Sewers." *Journal of Hydraulic Engineering* 129(4): 298-307.
638 https://doi.org/10.1061/(ASCE)0733-9429(2003)129:4(298)

639 Schaffner, J., and Steinhardt, J. 2006. "Numerical investigation of the self-acting flushing
640 system HydroFlush GS in Frankenberg/Germany." Paper presented at the 2th
641 Conference on Sewer Operation and Maintenance, Vienna, October.

642 Shahsavari, G., Arnaud-Fassetta, G., and Campisano, A. 2017. "A field experiment to
643 evaluate the cleaning performance of sewer flushing on non-uniform sediment
644 deposits." *Water Research* 118: 59–69 https://doi.org/10.1016/j.watres.2017.04.026

645 Shirazi, R., Campisano, A., Modica, C., and Willems, P. 2014. "Modelling the erosive
646 effects of sewer flushing using different sediment transport formulae." *Water*
647 *Science and Technology* 69(6): 1198–1204. https://doi.org/10.2166/wst.2013.810

648 Wan Mohtar, W., Afan, H., El-Shafie, A., Bong, C., and Ab Ghani, A. 2018. "Influence

649 of bed deposit in the prediction of incipient sediment motion in sewers using
650 artificial neural networks." *Urban Water Journal* 15(4): 296-302.
651 https://doi.org/10.1080/1573062X.2018.1455880

652 Yang, H., Zhu, D., Zhang, Y., and Zhou, Y. 2019. "Numerical investigation on bottom
653 shear stress induced by flushing gate for sewer cleaning." *Water Science and*
654 *Technology* 80(2): 290–299. https://doi.org/10.2166/wst.2019.269

655 Yu, C., and Duan, J. 2014. "Two-Dimensional Finite Volume Model for Sediment
656 Transport in Unsteady Flow." *World Environmental and Water Resources Congress*
657 *2014*: 1432–1441. https://doi.org/10.1061/9780784413548.144

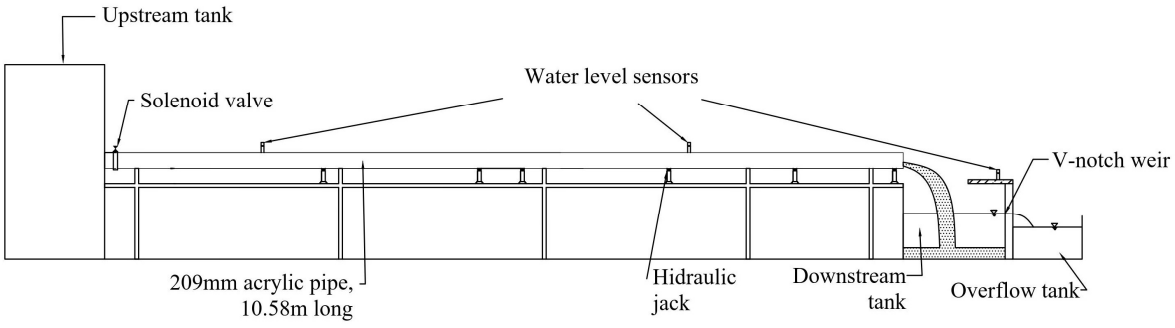

Figure 1. Experimental setup used to collect the unsteady flow data in the 209 mm acrylic pipe.

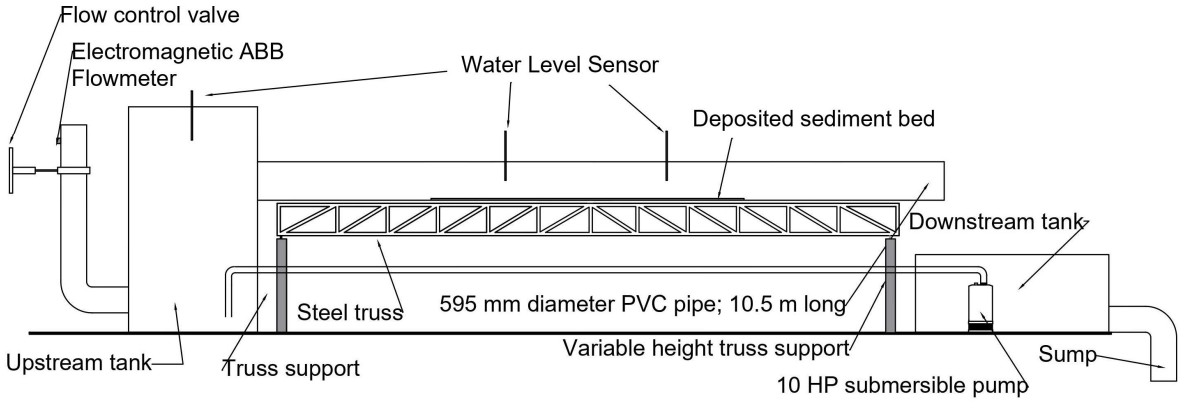

662

663 Figure 2. Experimental setup used to collect the unsteady flow data in the 595 mm PVC
664 pipe.

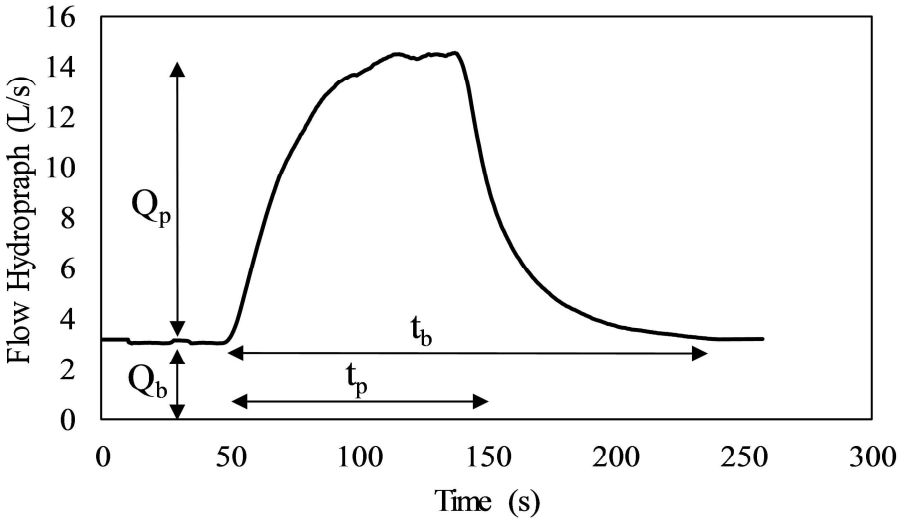

665

666 Figure 3. Variable definition of the flushing discharge hydrograph.

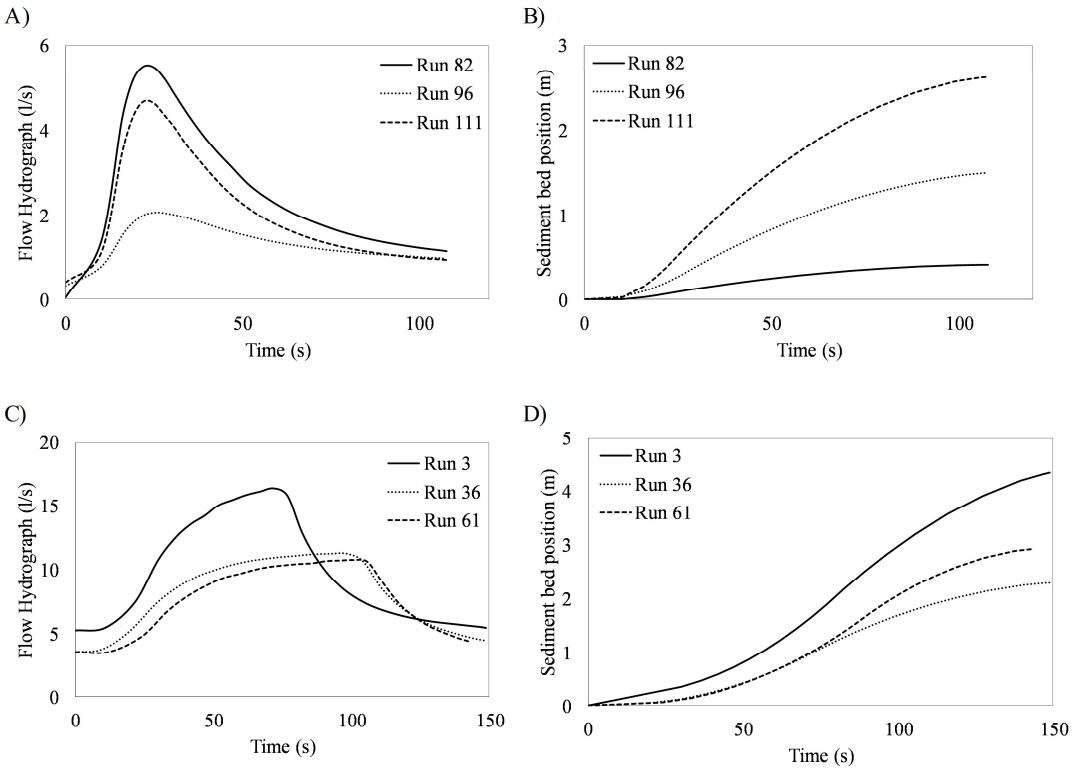

Figure 4. Example of flow hydrographs and sediment bed position for several experiments shown in Table 1.

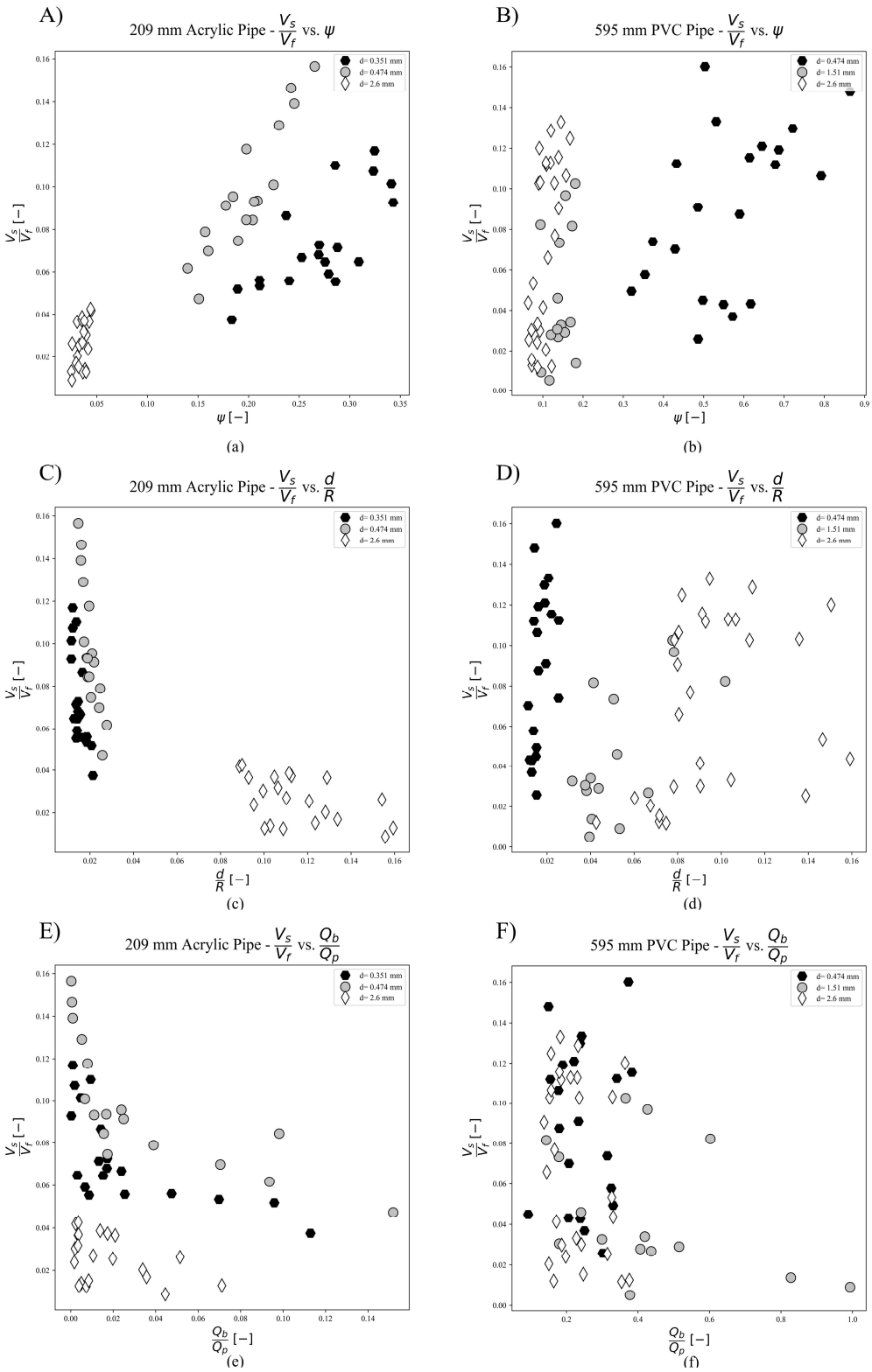

Figure 5. Plots showing the relationships between the dimensionless velocity (V_s/V_f) and other dimensionless variables in both acrylic and PVC pipe. Clustered results by particle diameter.

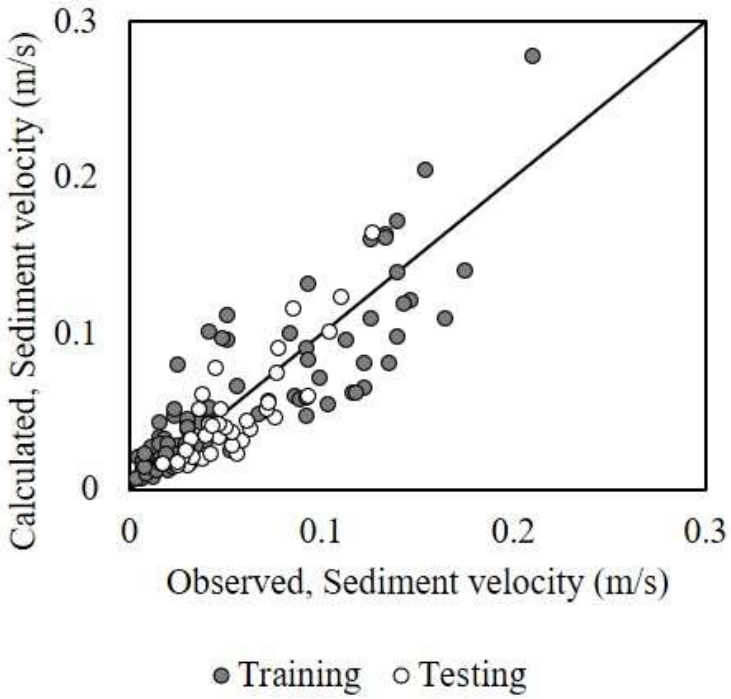

674

675 Figure 6. EPR-MOGA model accuracy for both training and testing stage.

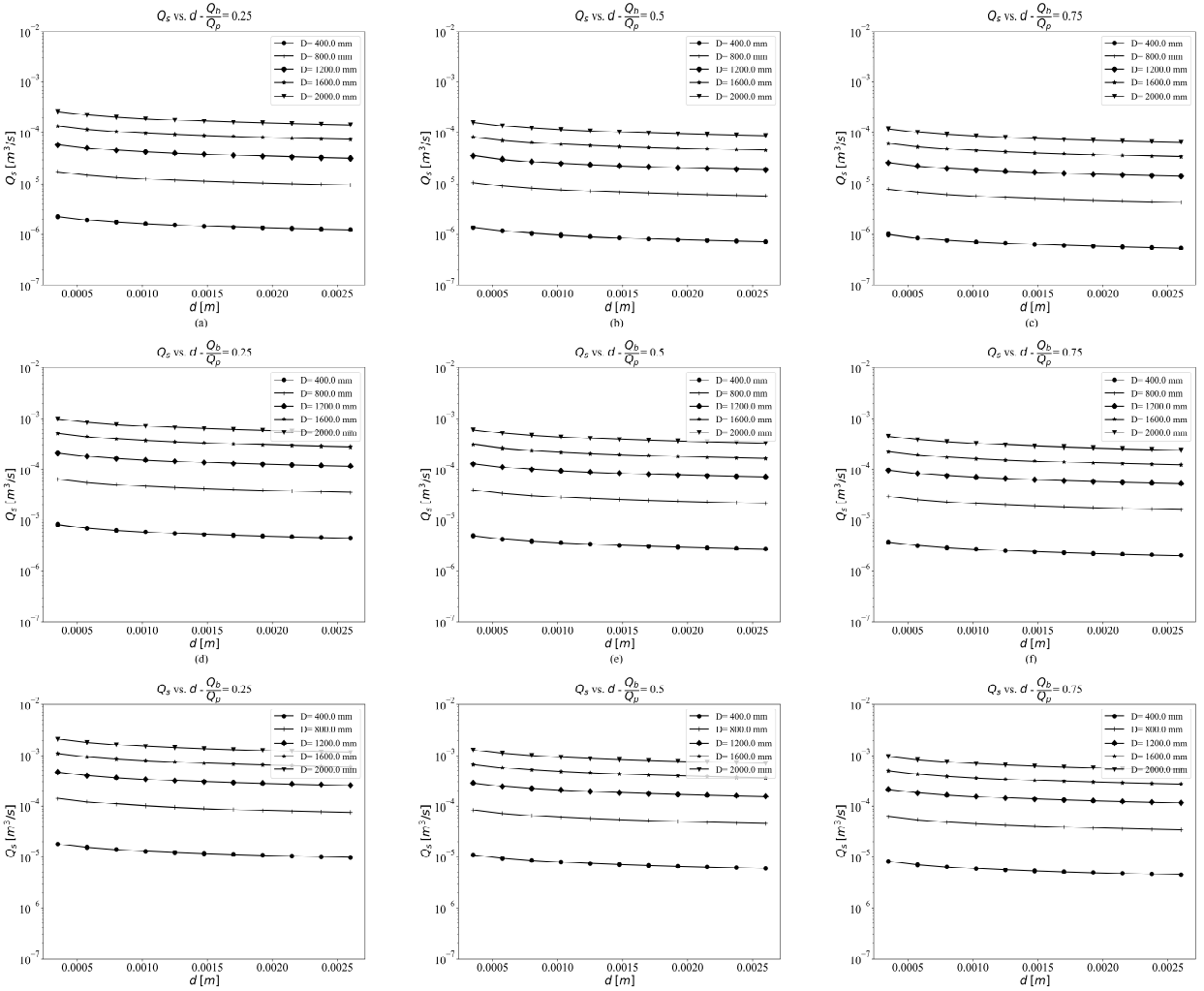

Figure 7. Efficiency of flushing discharge vs particle diameter for several base and peak flow relations ($0.25 < Q_b/Q_p < 0.75$) and pipe slope: a), b) and c) S_o = 0.5%; d), e) and f) S_o = 1.0% and g), h) and i) S_o = 1.5%.

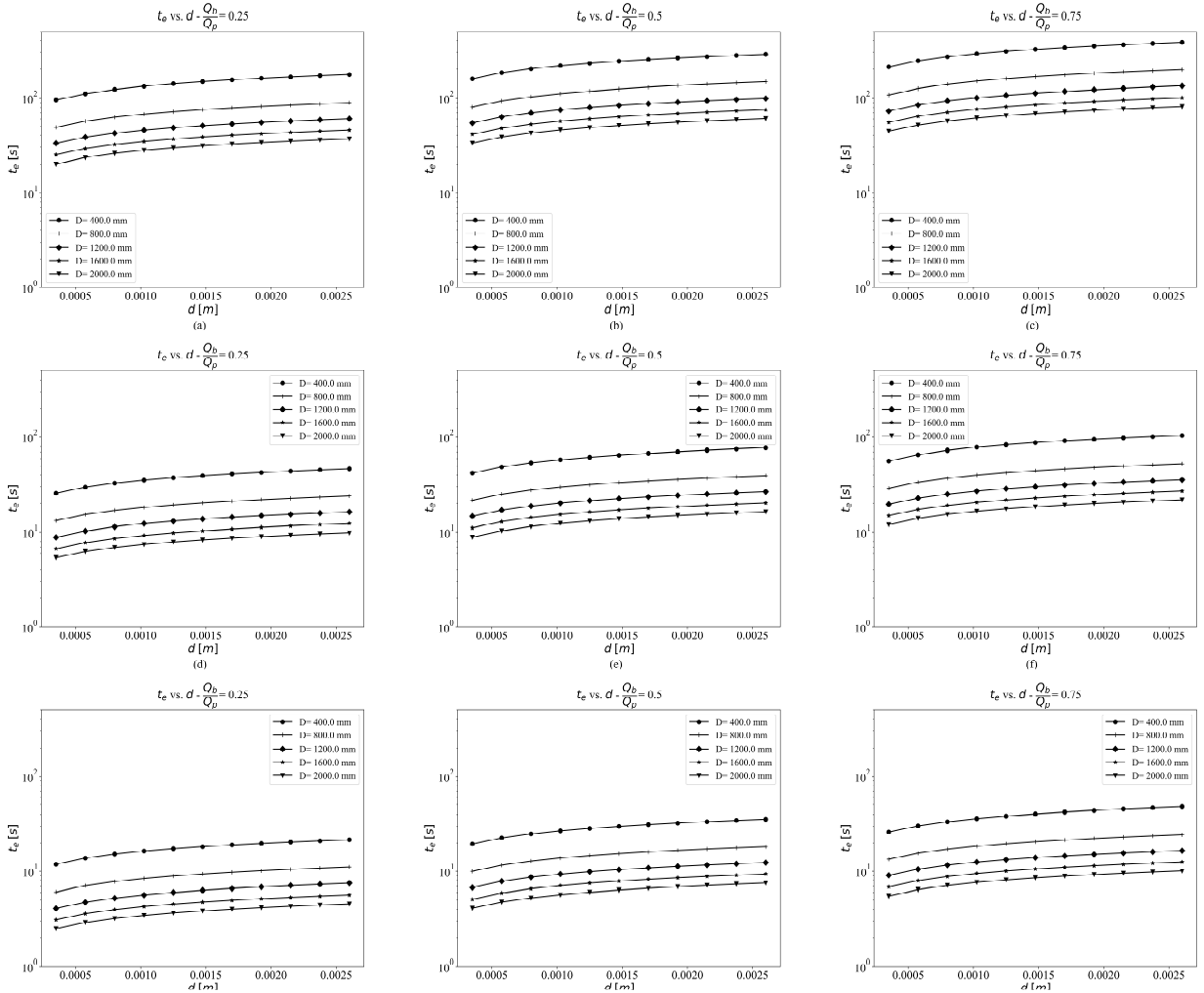

Figure 8. Flushing time vs particle diameter for several base and peak flow relations ($0.25 < Q_b/Q_p < 0.75$) and pipe slope: a), b) and c) S_o = 0.5%; d), e) and f) S_o = 1.0% and g), h) and i) S_o = 1.5%.

Table 1. Experimental data collected for studying flushing waves efficiency on sewer pipes.

Run no.	S_o (%)	D (mm)	Y (mm)	R (mm)	d (mm)	SG (-)	y_s (mm)	t_b (s)	t_p (s)	Q_b (l s^{-1})	Q_p (l s^{-1})	V_f (m s^{-1})	V_s (m s^{-1})
1	0.805	595	70.35	41.96	0.47	2.66	10.14	154	59	5.27	25.48	1.02	0.07
2	0.805	595	57.43	34.62	0.47	2.66	8.26	141	57	5.45	16.76	0.89	0.05
3	0.805	595	53.61	31.34	0.47	2.66	10.53	131	57	5.45	16.49	0.82	0.04
4	1.186	595	57.82	36.46	0.47	2.66	2.49	121	59	4.89	20.53	1.20	0.05
5	1.229	595	54.70	31.17	0.47	2.66	12.55	115	55	4.81	15.97	0.99	0.03
6	1.229	595	61.66	36.67	0.47	2.66	9.91	120	55	5.07	20.27	1.14	0.04
7	1.229	595	50.94	31.92	0.47	2.66	3.90	183	58	1.03	11.10	1.09	0.05
8	1.229	595	67.63	39.54	0.47	2.66	12.15	124	57	5.03	24.47	1.19	0.05
9	1.229	595	62.04	37.24	1.51	2.66	8.97	39	33	9.98	12.06	1.16	0.02
10	1.525	595	42.69	22.71	1.51	2.66	13.54	117	58	5.17	11.84	0.87	0.02
11	2.034	595	37.55	19.29	1.51	2.66	13.28	111	59	4.92	11.54	0.89	0.09
12	2.331	595	35.95	19.45	1.51	2.66	10.96	182	57	3.99	10.93	0.97	0.10
13	0.763	595	67.43	38.31	1.51	2.66	14.87	113	56	4.42	11.71	0.90	0.00
14	0.763	595	70.23	39.60	1.51	2.66	15.99	126	69	9.13	22.46	0.92	0.03
15	0.763	595	81.75	47.82	1.51	2.66	13.12	135	63	9.40	31.43	1.07	0.04
16	1.123	595	58.13	34.59	1.51	2.66	9.55	118	60	9.23	17.93	1.04	0.03
17	1.123	595	64.66	37.76	1.51	2.66	11.97	118	57	9.37	22.36	1.10	0.04
18	1.186	595	57.59	29.85	1.51	2.66	19.13	149	79	3.59	20.04	0.92	0.07
19	1.186	595	52.88	28.98	1.51	2.66	14.70	149	88	3.95	16.45	0.91	0.04
20	1.186	595	64.30	36.57	1.51	2.66	14.31	195	93	3.51	24.52	1.09	0.09
21	0.847	595	69.70	40.25	1.51	2.66	13.64	185	55	3.72	20.71	0.99	0.03
22	0.847	595	51.24	28.32	1.51	2.66	13.83	104	8	7.28	7.33	0.76	0.01
23	1.589	595	32.25	14.83	1.51	2.66	14.35	118	82	4.36	7.24	0.65	0.05
24	0.847	595	63.16	36.41	2.60	2.64	12.98	120	76	4.71	12.53	0.92	0.01
25	0.847	595	66.11	36.30	2.60	2.64	17.48	156	86	4.10	16.57	0.90	0.01
26	0.847	595	72.84	43.20	2.60	2.64	10.93	161	83	4.13	20.88	1.06	0.03
27	0.847	595	105.64	61.10	2.60	2.64	15.39	167	65	4.11	24.98	1.34	0.02
28	1.059	595	62.36	34.80	2.60	2.64	15.48	143	75	4.22	11.91	0.99	0.01
29	1.059	595	54.15	28.78	2.60	2.64	16.77	154	83	4.02	16.63	0.85	0.03
30	1.186	595	59.13	33.26	2.60	2.64	14.30	143	67	3.69	19.77	1.01	0.03
31	1.186	595	67.08	38.56	2.60	2.64	13.76	148	74	3.57	23.71	1.14	0.02
32	1.483	595	39.34	18.73	2.60	2.64	16.36	176	88	3.45	10.96	0.73	0.02

Run no.	S_o (%)	D (mm)	Y (mm)	R (mm)	d (mm)	SG (-)	y_s (mm)	t_b (s)	t_p (s)	Q_b (l s^{-1})	Q_p (l s^{-1})	V_f (m s^{-1})	V_s (m s^{-1})
33	1.483	595	46.74	24.88	2.60	2.64	14.66	136	80	3.52	15.45	0.91	0.03
34	1.483	595	53.25	28.81	2.60	2.64	15.54	186	72	3.39	19.73	1.01	0.04
35	1.483	595	59.57	32.28	2.60	2.64	16.95	184	79	3.42	23.61	1.10	0.07
36	1.653	595	38.51	16.34	2.60	2.64	19.13	134	82	3.75	11.36	0.69	0.03
37	1.653	595	46.08	23.02	2.60	2.64	17.21	141	84	3.76	15.96	0.90	0.09
38	1.653	595	52.56	28.02	2.60	2.64	16.18	146	70	3.71	20.08	1.04	0.12
39	1.653	595	59.13	33.13	2.60	2.64	14.58	147	64	3.64	23.79	1.19	0.12
40	1.568	595	38.73	18.76	0.47	2.66	15.60	135	87	3.64	11.58	0.76	0.06
41	1.568	595	46.16	24.41	0.47	2.66	14.80	142	81	3.73	15.96	0.92	0.08
42	1.568	595	53.90	29.62	0.47	2.66	14.77	146	87	3.66	20.35	1.07	0.09
43	1.568	595	59.10	34.08	0.47	2.66	12.39	151	81	3.75	24.25	1.20	0.13
44	1.822	595	37.55	18.70	0.47	2.66	14.29	140	87	4.06	11.92	0.82	0.09
45	1.822	595	45.29	22.96	0.47	2.66	16.33	148	88	4.00	16.48	0.95	0.13
46	1.822	595	51.59	29.70	0.47	2.66	11.33	152	81	3.95	20.87	1.17	0.14
47	2.034	595	35.08	19.49	0.47	2.66	9.71	121	84	3.97	10.64	0.92	0.15
48	2.034	595	42.85	24.99	0.47	2.66	9.05	161	89	3.26	14.75	1.11	0.13
49	2.034	595	50.35	30.68	0.47	2.66	6.79	7	78	3.56	20.07	1.32	0.14
50	2.034	595	54.22	33.47	0.47	2.66	5.64	178	60	3.56	23.79	1.42	0.21
51	2.246	595	34.90	21.54	0.47	2.66	4.68	127	75	4.36	11.38	1.09	0.13
52	2.246	595	42.64	25.31	0.47	2.66	7.95	159	77	3.78	15.90	1.19	0.15
53	2.246	595	35.17	17.28	2.60	2.64	13.82	131	78	4.07	11.19	0.86	0.10
54	2.246	595	42.78	22.75	2.60	2.64	13.58	142	88	3.62	15.55	1.06	0.14
55	2.246	595	47.24	27.46	2.60	2.64	9.96	146	85	3.62	19.82	1.24	0.17
56	2.246	595	52.77	31.74	2.60	2.64	8.10	142	79	3.72	23.74	1.40	0.18
57	2.076	595	36.93	19.14	2.60	2.64	12.77	136	85	3.90	11.87	0.90	0.09
58	2.076	595	43.16	24.38	2.60	2.64	10.84	11	77	3.69	16.02	1.09	0.12
59	2.076	595	50.20	28.50	2.60	2.64	11.99	153	92	3.67	20.34	1.21	0.14
60	2.076	595	54.70	32.31	2.60	2.64	9.85	154	79	3.79	24.16	1.35	0.14
61	1.822	595	36.34	17.74	2.60	2.64	14.46	123	84	3.54	10.84	0.79	0.04
62	1.822	595	43.56	25.20	2.60	2.64	9.63	162	85	3.20	15.12	1.05	0.12
63	1.822	595	50.97	30.34	2.60	2.64	8.79	171	78	3.18	19.05	1.21	0.09
64	1.822	595	56.21	32.54	2.60	2.64	11.66	168	87	3.25	23.71	1.25	0.11
65	0.644	209	34.99	20.17	2.60	2.64	5.60	101	18	0.08	3.80	0.55	0.02
66	0.644	209	49.27	27.29	2.60	2.64	8.22	101	16	0.01	6.60	0.68	0.02

Run no.	S_o (%)	D (mm)	Y (mm)	R (mm)	d (mm)	SG (-)	y_s (mm)	t_b (s)	t_p (s)	Q_b (l s^{-1})	Q_p (l s^{-1})	V_f (m s^{-1})	V_s (m s^{-1})
67	0.644	209	51.63	27.99	2.60	2.64	9.89	101	14	0.02	6.84	0.68	0.02
68	0.644	209	28.15	16.32	2.60	2.64	4.98	101	20	0.14	1.99	0.48	0.01
69	0.644	209	30.78	16.70	2.60	2.64	7.96	101	19	0.11	2.45	0.47	0.00
70	0.644	209	40.49	23.10	2.60	2.64	6.26	101	17	0.08	4.73	0.61	0.02
71	0.644	209	53.26	29.33	2.60	2.64	8.49	101	15	0.02	7.37	0.71	0.03
72	0.644	209	35.58	20.28	2.60	2.64	6.26	101	20	0.12	3.62	0.55	0.01
73	0.644	209	40.61	23.32	2.60	2.64	5.82	101	18	0.06	4.58	0.62	0.02
74	0.644	209	45.95	25.29	2.60	2.64	8.76	101	17	0.03	5.42	0.64	0.01
75	0.644	209	52.17	28.92	2.60	2.64	7.96	101	16	0.03	7.22	0.71	0.03
76	0.644	209	29.87	16.87	2.60	2.64	6.26	101	21	0.11	2.06	0.48	0.01
77	0.644	209	33.61	19.44	2.60	2.64	5.39	101	19	0.10	2.75	0.54	0.01
78	0.644	209	44.28	24.82	2.60	2.64	7.45	101	18	0.02	5.17	0.64	0.02
79	0.644	209	47.12	26.13	2.60	2.64	8.22	101	18	0.01	5.90	0.66	0.02
80	0.644	209	38.03	21.54	2.60	2.64	6.72	101	19	0.08	3.80	0.58	0.01
81	0.644	209	41.49	23.59	2.60	2.64	6.49	101	18	0.05	4.59	0.62	0.02
82	0.644	209	43.13	23.90	2.60	2.64	8.22	101	17	0.04	5.55	0.61	0.01
83	0.644	209	44.99	24.43	2.60	2.64	9.60	101	16	0.02	6.11	0.62	0.02
84	0.644	209	38.93	21.05	2.60	2.64	9.31	101	18	0.04	4.51	0.55	0.01
85	0.644	209	47.10	25.93	2.60	2.64	8.76	101	17	0.02	5.83	0.65	0.01
86	0.644	209	38.30	22.59	0.47	2.66	3.91	101	17	0.10	4.36	0.62	0.06
87	0.644	209	51.25	29.60	0.47	2.66	3.68	101	16	0.00	7.36	0.76	0.11
88	0.644	209	52.44	29.99	0.47	2.66	4.65	101	15	0.01	7.64	0.75	0.10
89	0.644	209	29.07	17.09	0.47	2.66	4.40	101	19	0.21	2.22	0.50	0.03
90	0.644	209	33.05	19.59	0.47	2.66	3.91	101	17	0.19	2.65	0.56	0.04
91	0.644	209	41.19	24.21	0.47	2.66	3.86	101	18	0.04	4.99	0.65	0.08
92	0.644	209	56.85	32.46	0.47	2.66	3.51	101	15	0.00	8.02	0.81	0.13
93	0.644	209	39.63	23.20	0.47	2.66	4.40	101	17	0.07	4.08	0.62	0.05
94	0.644	209	43.42	25.52	0.47	2.66	3.46	101	17	0.08	4.99	0.68	0.06
95	0.644	209	47.40	27.47	0.47	2.66	4.21	101	16	0.04	5.56	0.71	0.07
96	0.644	209	30.86	18.45	0.47	2.66	3.46	101	19	0.32	2.08	0.54	0.03
97	0.644	209	32.77	19.21	0.47	2.66	4.59	101	20	0.11	2.80	0.54	0.04
98	0.644	209	42.21	24.97	0.47	2.66	3.03	101	19	0.41	4.22	0.67	0.06
99	0.644	209	37.41	21.71	0.47	2.66	5.18	101	19	0.09	3.79	0.59	0.05
100	0.644	209	41.66	24.19	0.47	2.66	4.86	101	17	0.07	4.63	0.64	0.05

Run no.	S_o (%)	D (mm)	Y (mm)	R (mm)	d (mm)	SG (-)	y_s (mm)	t_b (s)	t_p (s)	Q_b (l s^{-1})	Q_p (l s^{-1})	V_f (m s^{-1})	V_s (m s^{-1})
101	0.644	209	43.34	25.14	0.47	2.66	4.78	101	18	0.06	5.71	0.66	0.06
102	0.644	209	48.65	28.13	0.47	2.66	4.21	101	16	0.03	6.67	0.72	0.09
103	0.644	209	36.32	21.27	0.35	2.65	4.59	101	18	0.06	4.24	0.58	0.05
104	0.644	209	51.00	29.01	0.35	2.65	5.60	101	15	0.01	6.81	0.73	0.08
105	0.644	209	50.99	29.11	0.35	2.65	5.18	101	15	0.01	6.90	0.73	0.09
106	0.644	209	28.62	16.45	0.35	2.65	5.39	101	18	0.23	2.00	0.48	0.02
107	0.644	209	32.66	18.92	0.35	2.65	5.26	101	17	0.19	2.67	0.53	0.03
108	0.644	209	42.79	24.72	0.35	2.65	5.18	101	16	0.07	4.80	0.65	0.04
109	0.644	209	54.41	30.76	0.35	2.65	5.60	101	17	0.00	7.36	0.76	0.07
110	0.644	209	37.13	21.55	0.35	2.65	5.18	101	18	0.10	3.75	0.59	0.03
111	0.644	209	41.56	24.21	0.35	2.65	4.59	101	17	0.08	4.71	0.64	0.05
112	0.644	209	45.08	25.81	0.35	2.65	5.73	101	17	0.07	5.47	0.67	0.05
113	0.644	209	54.08	30.60	0.35	2.65	5.60	101	15	0.03	7.31	0.76	0.08
114	0.644	209	29.46	16.96	0.35	2.65	5.39	101	20	0.19	2.02	0.49	0.03
115	0.644	209	33.04	18.92	0.35	2.65	5.90	101	19	0.13	2.74	0.53	0.03
116	0.644	209	44.81	25.64	0.35	2.65	5.82	101	17	0.04	5.18	0.66	0.04
117	0.644	209	48.43	27.71	0.35	2.65	5.39	101	17	0.02	5.88	0.70	0.05
118	0.644	209	39.31	22.65	0.35	2.65	5.60	101	18	0.09	3.92	0.60	0.04
119	0.644	209	41.99	24.16	0.35	2.65	5.60	101	17	0.08	4.59	0.63	0.04
120	0.644	209	43.59	25.04	0.35	2.65	5.60	101	18	0.04	5.64	0.65	0.04
121	0.644	209	44.65	25.62	0.35	2.65	5.60	101	17	0.06	6.12	0.66	0.07

Table 2. Pareto solution provided by the EPR-MOGA strategy.

Number of Inputs	Terms of monomial formula							Performance Index	
	Coefficient (a_j)	ψ	$\frac{Q_b}{Q_p}$	$\frac{d}{R}$	$\frac{y_s}{R}$	$\frac{t_b}{t_p}$	β	BIC	R^2
1	0.17	0.50	-	-	-	-	-	-48.21	0.38
2	0.14	0.60	-0.10	-	-	-	-	-66.19	0.48
3	8.13	1.40	-0.30	0.90	-	-	-	-104.55	0.63
4	11.47	1.50	-0.30	1.00	0.10	-	-	-100.56	0.64
5	121.48	2.10	-0.20	1.60	0.80	0.10	-	-96.49	0.64
6	2.48	1.40	-0.30	0.90	0.10	-0.20	1.00	-92.22	0.64

Table 3. Comparison of results for predicting the flushing efficiency in Laplace et al. (2003) case of study.

Reference	Removal rate [kg m^{-3}]	Observations
Laplace et al. (2003)	0.93	Original case of Study reported in a trunk combined sewer in Marseille, France
Dettmar (2007)	-	Volume of water value reported to clean a pipe section of 150 m long. Relevant parameters as pipe slope and particle diameter are not considered.
Bong et al. (2013)	0.21	Good approximation. Experimental model (Eq. (3)) obtained with a constant flume slope of 0.001.
EPR-MOGA Eq. (10)	0.4 – 1.25	Good performance for predicting the removal rate during flushing waves operation. Model consider relevant parameters as the mean particle diameter and the pipe geometry.